CrossMark

DIAGNOSTIC NEURORADIOLOGY

Quantitative T2, T2*, and T2′ MR imaging in patients with ischemic leukoaraiosis might detect microstructural changes and cortical hypoxia

Marlies Wagner[1] · **Michael Helfrich**[1] · **Steffen Volz**[2] · **Jörg Magerkurth**[1] · **Stella Blasel**[1] · **Luciana Porto**[1] · **Oliver C. Singer**[3] · **Ralf Deichmann**[2] · **Alina Jurcoane**[1] · **Elke Hattingen**[1]

Abstract

Introduction Quantitative MRI with T2, T2*, and T2′ mapping has been shown to non-invasively depict microstructural changes (T2) and oxygenation status (T2* and T2′) that are invisible on conventional MRI. Therefore, we aimed to assess whether T2 and T2′ quantification detects cerebral (micro-)structural damage and chronic hypoxia in lesions and in normal appearing white matter (WM) and gray matter (GM) of patients with ischemic leukoaraiosis (IL). Measurements were complemented by the assessment of the cerebral blood flow (CBF) and the degree of GM and WM atrophy.

Methods Eighteen patients with IL and 18 age-matched healthy controls were included. High-resolution, motion-corrected T2, T2*, and T2′ mapping, CBF mapping (pulsed arterial spin labeling, PASL), and segmentation of GM and WM were used to depict specific changes in both groups. All parameters were compared between patients and healthy controls, using t testing. Values of $p < 0.05$ were accepted as statistically significant.

Results Patients showed significantly increased T2 in lesions ($p < 0.01$) and in unaffected WM ($p = 0.045$) as well as significantly increased T2* in lesions ($p = 0.003$). A significant decrease of T2′ was detected in patients in unaffected WM ($p = 0.027$), while no T2′ changes were observed in GM ($p = 0.13$). Both unaffected WM and GM were significantly decreased in volume in the patient-group ($p < 0.01$). No differences of PASL-based CBF could be shown.

Conclusion Non-invasive quantitative MRI with T2, T2*, and T2′ mapping might be used to detect subtle structural and metabolic changes in IL. Assessing the grade of microstructural damage and hypoxia might be helpful to monitor disease progression and to perform risk assessment.

Alina Jurcoane and Elke Hattingen contributed equally to this work.

✉ Marlies Wagner
   marlies.wagner@kgu.de

1   Institute of Neuroradiology, University Hospital, Goethe-University, Schleusenweg 2-16, D-60528 Frankfurt am Main, Frankfurt, Germany

2   Brain Imaging Center, University Hospital, Goethe-University, Frankfurt, Germany

3   Department of Neurology, University Hospital, Goethe-University, Frankfurt, Germany

Introduction

Ischemic leukoaraiosis (IL) is a cerebral small vessel disease defined as a combination of diffuse white matter (WM) lesions (leukoaraiosis) and a history of clinical lacunar stroke [1]. The WM changes appear as hyperintense lesions in T2-weighted (T2w) MR images. Furthermore, there is evidence of histopathological rarefaction of myelin and axons due to alterations of the small penetrating arteries and arterioles, of the veins, and microcirculatory disturbances as well as activation of the coagulation-fibrinolysis pathway [2–6]. The alterations of small arteries and veins result in increased vessel length and narrowed lumina, yielding a decrease of perfusion pressure and cerebral blood flow (CBF) [1, 3, 5, 7–14]. Although a subsequent increase of the oxygen extraction fraction (OEF) partly compensates for the CBF reduction [15], there is a higher risk of hypoxia.

Cerebral small vessel disease clinically manifests as lacunar stroke with focal neurological deficits, being the most common cause of vascular dementia [7, 11, 12, 14, 16–25]. However, the correlation between the lesion load, as assessed from conventional T2w MR images, and clinical parameters remains weak [1, 11, 12, 16, 26–28]. Moreover, increased signal intensity in standard MRI may reflect a spectrum of pathological abnormalities ranging from very mild tissue changes to complete demyelination and axonal loss [12].

In contrast to conventional MRI, quantitative MRI techniques are more sensitive to microstructural and metabolic changes in brain tissue and might therefore differentiate between normal age-related white matter changes and potentially harmful changes due to small vessel disease [12, 14, 16, 27, 29–33].

The transverse relaxation time of blood water strongly depends on blood oxygenation, as spin dephasing induced by magnetic field distortions around erythrocytes increases in the presence of paramagnetic deoxygenated hemoglobin (deoxyHb). The resulting magnetic susceptibility differences between blood vessels and surrounding tissue reduce the effective transverse relaxation time T2*, and thus the signal in T2*-weighted images. However, T2* is also affected by changes of the transverse relaxation time T2, which increases in the cerebral cortex and thalami with age and in many cerebral pathologies due to edema or gliosis. To account for this effect, the relaxation time T2′ may be calculated from $1/T2' = 1/T2* - 1/T2$. T2′ provides mainly information about local concentrations of deoxyHb [34–36].

High-resolution, motion-corrected quantitative mapping of T2, T2*, and T2′ depicts microstructural changes and the oxygenation status in healthy individuals of younger and older ages [15, 37] and in patients with high-grade stenosis of intracranial arteries [38]. Likewise, combined mapping of the different transverse relaxation times T2, T2* and T2′ should also help to assess the grade of (micro-)structural damage (T2) and hypoxia (T2′), even in the normal appearing WM and gray matter (GM) of patients with IL. Here, respective mapping techniques were combined with pulsed arterial spin labeling (PASL)-based perfusion mapping of cortical CBF and quantification of cortical GM and WM atrophy to gather a more complete picture of IL.

Methods

Subjects

Eighteen patients with IL (age range 46–89 years; mean 71 years) were recruited via the local Department of Neurology. Inclusion criteria were as follows: (1) extensive WM lesions on conventional CT or MRI (Fazekas grade II or III) and (2) a recent (<2 weeks) clinical history of lacunar stroke.

Furthermore, 18 age-matched healthy controls (age range 46–88 years; mean 67 years; comparison with patients, $p = 0.215$) were included in the study. Controls were required to show no or only mild WM lesions (Fazekas grade 0 or I), and to have no clinical history of stroke [21]. Standardized questionnaires and medical records were used to exclude other neurologic or psychiatric diseases including manifested dementia, diabetes, or untreated hypertension in both groups.

The study protocol was approved by the Ethics Committee, Faculty of Medicine, Goethe University Frankfurt, and informed consent was obtained from each subject.

MR examination

Scans were performed on a 3-T MR scanner (Magnetom Trio; Siemens Medical Solutions, Erlangen, Germany), equipped with an eight-channel phased-array head coil for signal reception and a body coil for radio frequency (RF) transmission.

As described in detail elsewhere [15, 37], for quantitative T2* mapping, a multiple gradient echo sequence with eight echoes per excitation acquired exclusively under positive readout gradient polarity [39] was employed with the following imaging parameters: TE ranging from 10 to 52 ms with a constant increment of 6 ms, TR=3000 ms, 50 axial slices with 2 mm slice thickness, no interslice gap, bandwidth=300 Hz/pixel, excitation angle 30°, matrix size 160×128 (readout × phase encoding), field of view (FoV) 200×160 mm^2, isotropic spatial in-plane resolution of 1.25×1.25 mm^2, measurement time 6 min 24 s. To avoid erroneous T2* values due to distortions of the static magnetic field B0 [40–42], a compensation method was applied, based on obtaining B0 maps directly from the complex image data and correcting for TE-dependent image intensity reductions induced by spin dephasing [43]. The acquisition was repeated with 50 % spatial resolution in phase encoding direction (duration 3 min 30 s), and a special combination of both data sets in k-space was performed for the suppression of motion-induced artifacts [44].

Quantitative T2 mapping was based on the acquisition of a series of T2-weighted images with different values of TE (17, 86, 103, 120, 188 ms) but otherwise identical imaging parameters, using a turbo spin echo (TSE) sequence with TR=10 s, bandwidth=100 Hz/pixel, turbo factor=11. The relevant geometrical parameters (slice coverage and in-plane resolution) were identical to the T2* mapping experiment. The duration of each single T2-weighted data set was 2 min 22 s, so the total duration of T2 mapping was 11 min 50 s. Before T2 fitting, the TSE images were coregistered to the first T2*-weighted image using the linear registration algorithm implemented in FSL (FLIRT, FMRIB's Software Library-FSL, http://www.fmrib.ox.ac.uk/fsl). Data fitting was performed with custom-built programs written in MATLAB (MATLAB, The Mathworks Inc., Natick/MA, USA), using mono-exponential fitting for

obtaining maps of T2* and T2. Maps of T2′ were calculated as $1/T2'=1/T2^{*}-1/T2$.

Anatomical imaging was based on a T1-weighted MPRAGE sequence [45] with the following imaging parameters: TR/TE/TI=2250 ms/2.6 ms/900 ms, FoV 256×224×144 mm^3, whole brain coverage, isotropic spatial resolution 1 mm, 22 % oversampling in slice encoding (left-right) direction to avoid aliasing, bandwidth=200 Hz/pixel, excitation angle 9°, duration 7:23 min. This data set was used for segmentation of GM and WM. The fitted maps (T2, T2*, and T2′) were linearly coregistered to the T1-weighted anatomical data set using FLIRT. A 3D fluid attenuation inversion recovery (FLAIR) scan was also acquired to better differentiate lesions from normal appearing WM, GM, or cerebrospinal fluid (CSF), using the parameters TR/TE/TI=6000 ms/353 ms/2200 ms, FoV 250×215×160 mm^3, whole brain coverage, isotropic spatial resolution 1 mm, bandwidth=930 Hz/pixel, duration 8:08 min.

For quantitative measurement of brain perfusion, PASL-based CBF maps were acquired in 15 patients and 15 age-matched controls, sampling 100 pairs of control and tag images. Labeling was based on Q2TIPS (quantitative imaging of perfusion using a single subtraction, second version with interleaved thin-slice TI periodic saturation) as described by Luh et al. [46]. The proximal inversion with a control for off resonance effects (PICORE) labeling scheme was applied, labeling arterial spins inside a thick inversion slab proximal to the imaging slices. The scanning parameters were as follows: field of view (FOV)=240×240 mm^2, matrix size=64×64, isotropic in-plane resolution of 3.75×3.75 mm^2, five axial slices with 6 mm thickness placed at the centrum semiovale (Figs. 1 and 2), interslice gap of 2 mm, TR=2500 ms, TE=21 ms, TI1/TI1stop/TI2=700 ms/1375 ms/1400 ms, bandwidth=2694 Hz/pixel. The gap between the tag inversion slab and the first of the imaging slices was 10 mm. The duration was 8:20 min.

Hyperintense lesions were manually delineated as regions of interest (ROIs) on the FLAIR data set and were further coregistered to the T1-weighted anatomical data. Due to the limited field of view (five slices) in the case of PASL, coregistration to the reference anatomical images was not possible; thus, differentiation of CBF in cortex and subcortical structures was not possible, and PASL-GM ROIs had to be defined directly on the calculated CBF maps (Figs. 1 and 2).

Cortical GM and whole WM ROIs were defined following automatic segmentation with SPM 8 (http://www.fil.ion.ucl.ac.uk/spm) of the T1-weighted data set by classifying each voxel as either GM, WM, or CSF, depending on the highest probability value in the respective tissue maps, and excluding the lesions ROIs. Manually (lesions) and automatically (WM and GM) derived ROIs were used as masks to extract T2, T2*, and T2′ values from the corresponding maps, while the PASL-
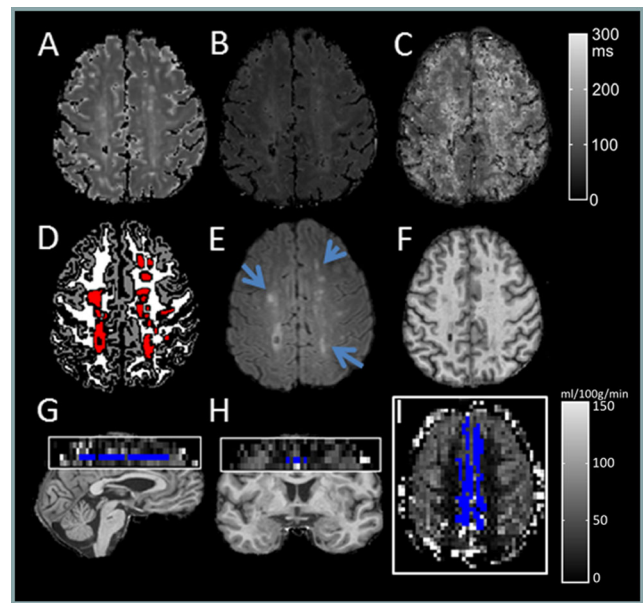
Fig. 1 MR images from a patient. *Upper row* shows T2 (*A*), T2* (*B*), and T2′ (*C*) maps. Regions of interest used in the study (*D*): lesions (*red*) are manually drawn on the FLAIR images (*E, arrows*), while gray matter (*gray*) and white matter (*white*) are automatically segmented based on T1-weighted (T1-w) images (*F*). An additional region of interest (*blue*) was manually drawn on the CBF maps (PASL) (*I*) on five slices at the level of the centrum semiovale as demonstrated on sagittal (*G*) and coronal (*H*) views (overlapped on T1w image). Note the inhomogeneous gray values distribution of the quantitative maps that makes visual assessment difficult and demonstrates the necessity of quantitative evaluation. This slice is compatible with patient's group results of T2 and T2* values but is an outlier for T2′ values in the lesions and the GM (higher than group results)
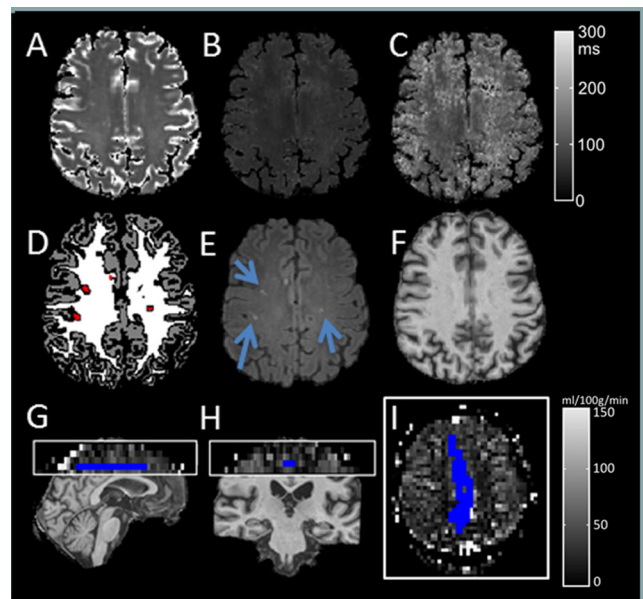
Fig. 2 MR images from a control subject. Panel's description as in Fig. 1. This slice is compatible with controls' group results for T2* and T2′ values but is an outlier for T2 values in the lesions and the GM (higher than group results)

GM ROI was used to extract PASL-based CBF values (Figs. 1 and 2).

Relative volume fractions of GM, WM, and lesions were calculated, dividing the respective volume by the total intracranial volume (the latter being calculated as the combined volume of GM, WM, CSF, and lesions). It should be noted that GM, WM, or CSF compartments were defined as mutually exclusive regions, each voxel being assigned to one tissue class with exclusion of the manually defined lesion ROIs as explained above.

All parameters derived as described above were compared between patients and healthy controls using t testing. Statistical comparison was performed by means of the software R Statistics 2.15. Values of $p < 0.05$ were accepted as statistically significant.

Results

Within the lesions and the unaffected WM, the T2 relaxation time was significantly increased in patients as compared to controls ($p < 0.01$ and $p = 0.045$, respectively). In GM, there were no T2 differences.

The T2* relaxation time was significantly increased in the patients as compared to controls in the lesions ($p = 0.003$). However, there were no T2* differences in WM or GM.

T2′ was significantly decreased in normal appearing WM of patients ($p = 0.027$). In contrast, there were no T2′ alterations in patients' GM as compared to controls (Table 1).

No changes could be found in the PASL-based CBF in GM between patients and controls (53.06 ± 21.85 ml/100 g/min and 48.43 ± 12.87 ml/100 g/min, respectively, $p = 0.49$). However, it is worth noting that the statistical scattering was smaller in the control group.

As expected from inclusion criteria, the lesion fraction was significantly larger in patients than that in controls ($p < 0.01$). Patients showed a significant smaller fraction of normal appearing WM and GM (lesions excluded) than controls ($p < 0.01$) (Table 2).

Discussion

This study employed quantitative T2, T2*, and T2′ mapping, PASL-based perfusion mapping, and WM-GM segmentation to assess (micro-)structural damage and hypoxia in lesions and normal appearing WM and GM in patients with IL compared with age-matched healthy controls.

Results (Table 1) show that in patients with IL, T2 is significantly increased both in lesions and in the normal appearing WM. In contrast, no T2 differences were found in GM.

Hyperintense lesions on standard T2-weighted MRI are rather unspecific and can reflect a spectrum of abnormalities, ranging from very mild tissue changes to complex demyelination and axonal loss in the presence of small vessel disease [12]. In patients with IL, WM lesions are caused by lacunar or incomplete infarction with a damage of myelin, axons, and astroglia [3–6, 29, 47]. In contrast, WM lesions appearing during normal aging [15, 33]—as in our control group—appear to be of non-vascular origin without tissue damage but with reduced myelination, atrophy of the neuropil, and enlarged perivascular spaces [6, 27]. While this difference is not sufficiently assessable via conventional MR imaging, quantitative T2 mapping might help to distinguish the nature of these lesions.

The observed T2 increase in the normal appearing WM (after lesion exclusion) of IL patients as compared to age-matched controls may be caused by diffuse WM damage with demyelination and microinfarcts in IL patients [4, 28]. Previous studies using quantitative T2 mapping revealed a T2 increase with age, even in healthy volunteers; however, WM lesions were not excluded from WM analysis in these studies [15, 33]. This global WM damage—even in the normal appearing WM—could already be demonstrated using different quantitative MR techniques, including magnetization transfer (MTR) mapping [27, 32] and diffusion tensor imaging (DTI) [12, 16, 29–31]. In these studies, changes of the normal appearing WM of patients with vascular changes corresponded to damaged ultrastructure even

Table 1 Values of relaxation times T2, T2*, and T2′ [ms], comparison between patients with IL and controls in three regions of interest: lesions, white matter (WM), and gray matter (GM)

		T2 [ms]	p value	T2*[ms]	p value	T2′ [ms]	p value
Lesions	Patients	143.66 ± 17.18	$<0.01*$	62.51 ± 6.66	$0.003*$	112.22 ± 16.41	0.8
	Controls	111.98 ± 9.19		56.32 ± 4.15		110.99 ± 10.95	
WM	Patients	103.25 ± 7.08	$0.045*$	50.09 ± 3.81	0.45	95.31 ± 14.65	$0.027*$
	Controls	99.12 ± 4.43		50.92 ± 2.55		105.24 ± 10.6	
GM	Patients	107.97 ± 11.07	0.753	46.16 ± 5.04	0.08	75.18 ± 17.61	0.13
	Controls	109.38 ± 15.36		49 ± 4.48		83.18 ± 13.09	

When present (all patients $n = 18$, some controls $n = 14$), lesions were manually drawn on FLAIR images. WM and GM were automatically segmented with SPM8. Significant differences ($p < 0.05$) are marked with asterisk

Table 2 Fractions of lesion, white matter (WM), and gray matter (GM) relative to total intracranial volume, comparison between IL patients and controls

	Patients	Controls	*p* value
Lesion fraction	0.06±0.02	0±0.01	<0.01*
WM fraction	0.29±0.02	0.32±0.02	<0.01*
GM fraction	0.45±0.01	0.47±0.01	<0.01*

outside of the visible lesions. Further, the observed changes correlated with clinical presentation. Assuming that T2 prolongation also reflects microstructural damage (see also below), quantitative T2 mapping might therefore be helpful to assess prognosis and to monitor therapeutic effects in patients with IL.

In the GM of patients, one might have expected an increase of T2 due to the parenchymal damage caused by cortical microinfarcts. However, no T2 alterations were found (Table 1), probably due to a good collateral supply saving the GM from substantial damage [4, 19, 28].

T2* was significantly increased in the lesions of IL patients as compared to controls, while no T2* changes were observed in the normal appearing WM or in the GM (Table 1). T2* is influenced by paramagnetic tissue properties (T2′) which primarily depend on heme-bound and ferritin-bound iron. However, T2* also depends on diamagnetic effects (T2), which are more marked in the WM and in patients with IL. To assess the paramagnetic tissue properties without the influence of T2 effects, T2′ should be used (see below) [15, 37, 48]. Since T2′ was unaltered in the lesions of patients as compared to controls, the significant increase of T2* in the lesions of patients is likely an effect of the locally increased T2.

In the GM, T2′ was similar in patients and in controls (Table 1). Again, the good collateral supply may save the GM from hypoxia in patients with IL [4, 19, 28].

However, in the unaffected WM, T2′ was significantly decreased in patients (Table 1). As T2′ decreases with increasing concentrations of paramagnetic deoxyHb, T2′ serves as a marker for hypoxia [15, 37, 38]. The decreased T2′ in the WM of patients with IL therefore seems to reflect the hypoxic state in their normal appearing WM. Misery perfusion might be one important factor contributing to hypoxia in IL patients. Due to pathologic changes of the small arteries and veins and the decreased vascular density in the WM of IL patients, the reduced hemodynamic response is not sufficient to meet the metabolic demands in the case of even small decreases in cerebral perfusion pressure. As a consequence, OEF increases [3, 10, 11]. An increased OEF along with reduced CBF, however, is associated with an increased risk of incomplete infarction

or stroke [3, 49, 50]. As described by Schmidt et al. [6], factors induced by hypoxia can be found in deep and subcortical WM lesions in patients with cerebral microangiopathy. Previous studies using positron emission tomography (PET) with different tracers showed partly contradictory results. While OEF was unaltered in patients with vascular dementia or non-demented patients with leukoaraiosis in some PET studies [17, 51], other authors reported OEF increases [10, 11]. Meguro [52] showed that OEF was higher in patients with severe periventricular hyperintensities (PVH) compared with those with mild or no PVH, although lacking statistical significance.

Therefore, the decrease of T2′ in normal appearing WM might be interpreted as a marker of hypoxia and might help to estimate the risk of new lesions in patients with IL. Furthermore, Yao et al. [11] stated that cognitive function in patients with vascular dementia does not directly correlate with the severity of WM lesions but rather with a decreased oxygen metabolism detected by PET. Therefore, T2′ mapping might also be useful to assess the risk of cognitive impairment in patients with IL.

Further, the observation of both increased T2 and decreased T2′ in the normal appearing WM might support the hypothesis of severe structural damage in patients with IL. Deoxygenation has a bearing on T2, and hypoxia leads to a T2 decrease, especially in the blood [53, 54]. However, tissue T2 is also influenced by certain pathologies such as the occurrence of edema or gliosis which yield a T2 increase. In contrast, T2′ is primarily affected by paramagnetic tissue properties and is therefore a more sensitive marker of hypoxia. If, as in this study presented here, both a decrease in tissue T2′ (as a marker of hypoxia) and an increase in tissue T2 are observed, the latter effect is likely to be caused by pathological tissue alterations that level out the decreasing effect of hypoxia on T2. Thus, the combination of increased T2 and decreased T2′ should indicate even more severe tissue damage.

We found no difference in cortical CBF between patients and controls on the basis of PASL-based CBF maps. Other studies found a cortical CBF decrease in IL patients with different imaging modalities including PET and MRASL [52, 55]. This discrepancy in results may be due to the use of different mapping techniques. It has been shown that PASL may lead to an overestimation of CBF in patients with small vessel disease like IL, which might be caused by stagnation of labeled blood in small vessel ectasia [56]. Furthermore, in the case of decreased perfusion pressure, cerebral autoregulation might induce a cerebral blood volume (CBV) increase which also might contribute to a PASL-based overestimation of CBF in IL. In our IL patients, PASL-based CBF values showed a wider scattering than for controls, probably

due to partial volume effects resulting from the significant decrease of cortical volume (see below) [56, 57]. Unfortunately, CBF in the WM cannot be reliably determined due to the low signal to noise ratio even at 3 T, which prevents detection of the almost fourfold lower perfusion in white matter relative to gray matter [37, 58]. However, it has been shown that there is a CBF decrease in WM of IL patients, and we speculate that this may also be true for our study [1, 3, 5, 7–14].

In fact, we found significantly lower GM and WM fractions in IL patients than those in controls (Table 2). This is in line with the results of previous studies that reported cortical atrophy in patients with leukoaraiosis and subcortical vascular disease [13, 59]. The mechanism of cortical atrophy in patients with IL is not yet fully elucidated and might be of primary or secondary nature [13, 18, 60]. Synaptic loss, apoptosis, necrosis, shrinkage, and decreased CBF [14, 18] as well as direct injury from microscopic cortical infarcts [60] might contribute to cortical thinning.

As a limitation, it has to be stated that non-heme-bound iron has a relevant impact on the paramagnetic tissue characteristics. Most human brain iron is found within the iron storage protein ferritin and its breakdown product, hemosiderin [61, 62]. For hypertensive patients, significantly higher iron content due to microbleeds has been reported [62]. In our study, patients with untreated hypertension were excluded both from the patient and the control group. Further, for patients and controls, there was no evidence of cerebral microbleeds in the acquired T2* maps. However, an additional impact of microbleeds on T2′ cannot be fully ruled out. Further, iron-rich amyloid plaques, which are contributors of non-heme iron in the aging brain [63], may have influenced T2′. However, the use of an age-matched control group should account for these age-related effects. Finally, it is worth noting that the more gradual reduction in oxygen consumption is accompanied by a slower increase in non-heme iron in the later decades [64]. T2′ should therefore be a useful tool to detect differences of deoxyHb in patients and controls of higher age.

Further, we lack additional supporting evidence from clinical correlations, since no neuropsychological testing was performed.

Conclusion

Non-invasive quantitative MRI with T2, T2*, and T2′ mapping may be used to detect structural and metabolic changes in ischemic leukoaraiosis. Assessing the grade of microstructural damage and hypoxia may be helpful to monitor disease progression and to perform a risk assessment.

References

1. Braffman BH, Zimmerman RA, Trojanowski JQ et al (1988) Brain MR: pathologic correlation with gross and histopathology. 1. Lacunar infarction and Virchow-Robin spaces. AJR Am J Roentgenol 151:551–558
2. Garcia JH (1997) Cognitive impairment and cellular/vascular changes in the cerebral white matter. Ann N Y Acad Sci 826:92–102
3. Brown WR, Thore CR (2011) Review: cerebral microvascular pathology in ageing and neurodegeneration. Neuropathol Appl Neurobiol 37:56–74
4. Brundel M, de Bresser J, van Dillen JJ et al (2012) Cerebral microinfarcts: a systematic review of neuropathological studies. Cereb Blood Flow Metab 32:425–436
5. Akiguchi I, Tomimoto H, Wakita H et al (1999) Cytopathological alterations and therapeutic approaches in Binswanger's disease. Neuropathology 19:119–128
6. Schmidt R, Schmidt H, Haybaeck J et al (2011) Heterogeneity in age-related white matter changes. Acta Neuropathol 122:171–185
7. O'Sullivan M, Lythgoe DJ, Pereira AC et al (2002) Patterns of cerebral blood flow reduction in patients with ischemic leukoaraiosis. Neurology 59:321–326
8. Jones DK, Lythgoe D, Horsfield MA et al (1999) Characterization of white matter damage in ischemic leukoaraiosis with diffusion tensor MRI. Stroke 30:393–397
9. Pantoni L, Garcia JH (1997) Pathogenesis of leukoaraiosis: a review. Stroke 28:652–659
10. Fujii K, Sadoshima S, Okada Y et al (1990) Cerebral blood flow and metabolism in normotensive and hypertensive patients with transient neurologic deficits. Stroke 21:283–290
11. Yao H, Sadoshima S, Ibayashi S et al (1992) Leukoaraiosis and dementia in hypertensive patients. Stroke 23:1673–1677
12. Schmidt R, Ropele S, Ferro J et al (2010) Diffusion-weighted imaging and cognition in the leukoariosis and disability in the elderly study. Stroke 41:e402–e408
13. Nitkunan A, Lanfranconi S, Charlton RA et al (2011) Brain atrophy and cerebral small vessel disease: a prospective follow-up study. Stroke 42:133–138
14. Duering M, Righart R, Csanadi E et al (2012) Incident subcortical infarcts induce focal thinning in connected cortical regions. Neurology 79:2025–2028
15. Wagner M, Jurcoane A, Volz S et al (2012) Age-related changes of cerebral autoregulation: new insights with quantitative T2′-mapping and pulsed arterial spin-labeling MR imaging. AJNR Am J Neuroradiol 33:2081–2087
16. Nitkunan A, Barrick TR, Charlton RA et al (2008) Multimodal MRI in cerebral small vessel disease: its relationship with cognition and sensitivity to change over time. Stroke 39:1999–2005

17. Yao H, Sadoshima S, Kuwabara Y et al (1990) Cerebral blood flow and oxygen metabolism in patients with vascular dementia of the Binswanger type. Stroke 21:1694–1699

18. Smith EE, Arboix A (2012) Focal cortical thinning is caused by remote subcortical infarcts: spooky action at a distance. Neurology 79:2016–2017

19. Ii Y, Maeda M, Kida H et al (2013) In vivo detection of cortical microinfarcts on ultrahigh-field. MRI J Neuroimag 23:28–32

20. Heiss WD, Zimmermann-Meinzingen S (2012) PET imaging in the differential diagnosis of vascular dementia. J Neurol Sci 322:268–273

21. Fazekas F, Chawluk JB, Alavi A et al (1987) MR signal abnormalities at 1.5 T in Alzheimer's dementia and normal aging. AJR Am J Roentgenol 149:351–356

22. Loizou LA, Kendall BE, Marshall J (1981) Subcortical arteriosclerotic encephalopathy: a clinical and radiological investigation. J Neurol Neurosurg Psychiatry 44:294–304

23. Kövari E, Gold G, Herrmann FR et al (2004) Cortical microinfarcts and demyelination significantly affect cognition in brain aging. Stroke 35:410–414

24. van Gijn J (1998) Leukoaraiosis and vascular dementia. Neurology 51(3 Suppl 3):S3–S8

25. Caplan LR (1995) Binswanger's disease—revisited. Neurology 45:626–633

26. The LADIS Study Group, Poggesi A, Pantoni L (2011) 2001–2011: a decade of the LADIS (Leukoaraiosis And DISability) study: what have we learned about white matter changes and small-vessel disease? Cerebrovasc Dis 32:577–588

27. Inglese M, Ge Y (2004) Quantitative MRI: hidden age-related changes in brain tissue. Top Magn Reson Imag 15:355–363

28. van Veluw SJ, Zwanenburg JJ, Engelen-Lee J et al (2013) In vivo detection of cerebral cortical microinfarcts with high-resolution 7T MRI. J Cereb Blood Flow Metab 33:322–329

29. Chabriat H, Pappata S, Poupon C et al (1999) Clinical severity in CADASIL related to ultrastructural damage in white matter: in vivo study with diffusion tensor MRI. Stroke 30:2637–2643

30. Sotak CH (2002) The role of diffusion tensor imaging in the evaluation of ischemic brain injury—a review. NMR Biomed 15:561–569

31. Jones DK, Lythgoe D, Horsfield MA et al (1999) Characterization of white matter damage in ischemic leukoaraiosis with diffusion tensor MRI. Stroke 30:393–397

32. Spilt A, Goekoop R, Westendorp RG et al (2006) Not all age-related white matter hyperintensities are the same: a magnetization transfer imaging study. AJNR Am J Neuroradiol 27:1964–1968

33. Siemonsen S, Finsterbusch J, Matschke J et al (2008) Age-dependent normal values of T2* and T2′ in brain parenchyma. AJNR Am J Neuroradiol 29:950–955

34. Thulborn KR, Waterton JC, Matthews PM, Radda GK (1982) Oxygenation dependence of the transverse relaxation time of water protons in whole blood at high field. Biochim Biophys Acta 714:265–270

35. Breger RK, Yetkin FZ, Fischer ME, Papke RA, Haughton VM, Rimm AA (1991) T1 and T2 in the cerebrum: correlation with age, gender, and demographic factors. Radiology 181:545–547

36. Ding XQ, Kucinski T, Wittkugel O et al (2004) Normal brain maturation characterized with age-related T2 relaxation times: an attempt to develop a quantitative imaging measure for clinical use. Invest Radiol 39:740–746

37. Wagner M, Magerkurth J, Volz S et al (2012) T2′- and PASL-based perfusion mapping at 3 Tesla: influence of oxygen-ventilation on cerebral autoregulation. J Magn Reson Imag 36:1347–1352

38. Seiler A, Jurcoane A, Magerkurth J et al (2012) T2′ imaging within perfusion-restricted tissue in high-grade occlusive carotid disease. Stroke 43:1831–1836

39. Williams DS, Detre JA, Leigh JS et al (1992) Magnetic resonance imaging of perfusion using spin inversion of arterial water. Proc Natl Acad Sci U S A89:212–216

40. Losert C, Peller M, Schneider P et al (2002) Oxygen-enhanced MRI of the brain. Magn Reson Med 48:271–277

41. Ericsson A, Weis J, Hemmingsson A et al (1995) Measurements of magnetic field variations in the human brain using a 3D-FT multiple gradient echo technique. Magn Reson Med 33:171–177

42. Ordidge RJ, Gorell JM, Deniau JC et al (1994) Assessment of relative brain iron concentrations using T2-weighted and T2*-weighted MRI at 3 Tesla. Magn Reson Med 32:335–341

43. Baudrexel S, Volz S, Preibisch C et al (2009) Rapid single-scan T2*-mapping using exponential excitation pulses and image-based correction for linear background gradients. Magn Reson Med 62:263–268

44. Magerkurth J, Volz S, Wagner M et al (2011) Quantitative T*2-mapping based on multi-slice multiple gradient echo flash imaging: retrospective correction for subject motion effects. Magn Reson Med 66:989–997

45. Mugler JP 3rd, Brookeman JR (1990) Three-dimensional magnetization-prepared rapid gradient-echo imaging (3D MP RAGE). Magn Reson Med 15:152–157

46. Luh WM, Wong EC, Bandettini PA et al (1999) QUIPSS II with thin-slice TI1 periodic saturation: a method for improving accuracy of quantitative perfusion imaging using pulsed arterial spin labeling. Magn Reson Med 41:1246–1254

47. Pantoni L, Garcia JH (1997) Cognitive impairment and cellular/vascular changes in the cerebral white matter. Ann N Y Acad Sci 826:92–102

48. Langkammer C, Krebs N, Goessler W et al (2012) Susceptibility induced grey-white matter MRI contrast in the human brain. Neuroimage 59:1413–1419

49. Kesavadas C, Santhosh K, Thomas B (2010) Susceptibility weighted imaging in cerebral hypoperfusion—can we predict increased oxygen extraction fraction? Neuroradiology 52:1047–1054

50. Derdeyn CP, Videen TO, Yundt KD et al (2002) Variability of cerebral blood volume and oxygen extraction: stages of cerebral haemodynamic impairment revisited. Brain 125:595–607

51. Frackowiak RS, Pozzilli C, Legg NJ et al (1981) Regional cerebral oxygen supply and utilization in dementia. A clinical and physiological study with oxygen-15 and positron tomography. Brain 104:753–778

52. Meguro K, Hatazawa J, Yamaguchi T et al (1990) Cerebral circulation and oxygen metabolism associated with subclinical periventricular hyperintensity as shown by magnetic resonance imaging. Ann Neurol 28:378–383

53. Thulborn KR, Waterton JC, Matthewa PM et al (1982) Oxygenation dependence of the transverse relaxation time of water protons in whole blood at high field. Biochimica et Biophysica Acta 714:265–270

54. Zhao JM, Clingman CS, Närväinen MJ et al (2007) Oxygenation and hematocrit dependence of transverse relaxation rates of blood at 3T. Magn Reson Med 58:592–597

55. Bastos-Leite AJ, Kuijer JP, Rombouts SA et al (2008) Cerebral blood flow by using pulsed arterial spin-labeling in elderly subjects with white matter hyperintensities. AJNR Am J Neuroradiol 29:1296–1301

56. Kamano H, Yoshiura T, Hiwatashi A et al (2013) Arterial spin labeling in patients with chronic cerebral artery steno-occlusive disease: correlation with (15)O-PET. Acta Radiol 54:99–106

57. Asllani I, Habeck C, Borogovac A et al (2009) Separating function from structure in perfusion imaging of the aging brain. Hum Brain Mapp 30:2927–2935

58. Bulte DP, Chiarelli PA, Wise RG et al (2007) Cerebral perfusion response to hyperoxia. J Cereb Blood Flow Metab 27:69–75

59. Akiyama H, Meyer JS, Mortel KF et al (1997) Normal human aging: factors contributing to cerebral atrophy. J Neurol Sci 152: 39–49

60. Launer LJ, Hughes TM, White LR (2011) Microinfarcts, brain atrophy, and cognitive function: the Honolulu Asia Aging Study Autopsy Study. Ann Neurol 70:774–780

61. Duyn JH, van Gelderen P, Li TQ et al (2007) High-field MRI of brain cortical substructure based on signal phase. Proc Natl Acad Sci U S A 104:11796–11801

62. Rodrigue KM, Haacke EM, Raz N (2011) Differential effects of age and history of hypertension on regional brain volumes and iron. Neuroimage 54:750–759

63. Collingwood JF, Chong RK, Kasama T et al (2008) Three-dimensional tomographic imaging and characterization of iron compounds within Alzheimer's plaque core material. J Alzheimers Dis 14:235–245

64. Hallgren B, Sourander P (1958) The effect of age on the non-haemin iron in the human brain. J Neurochem 3:41–51